

Article

Unveiling the Photocatalytic Activity of Carbon Dots/g-C₃N₄ Nanocomposite for the O-Arylation of 2-Chloroquinoline-3-carbaldehydes

Ravichandran Manjupriya and Selvaraj Mohana Roopan * 

Chemistry of Heterocycles & Natural Product Research Laboratory, Department of Chemistry, School of Advanced Sciences, Vellore Institute of Technology, Vellore 632 014, India

* Correspondence: mohanaroopan.s@vit.ac.in; Tel.: +0416-220-2313

Abstract: Visible-light-active, organic, heterogeneous photocatalysts offer an ecologically friendly and sustainable alternative to traditional metal-based catalysts. In this work, we report the microwave synthesis of nanocarbon dots (CDs), loaded with graphitic carbon nitride (g-C₃N₄). The fabricated nanocomposite was shown to exhibit various properties, such as the Schottky heterojunction. The optical properties, functional group analysis, surface morphology, crystallinity, chemical stability, electronic properties, and pore size distribution of the synthesized nanocomposite were analyzed by Ultraviolet-Diffuse Reflectance Spectroscopy (UV-DRS), Photoluminescence (PL), Fourier Transform Infrared Spectroscopy (FTIR), Transmission Electron Microscopy (TEM), X-Ray Diffraction (XRD), Zeta potential, X-Ray Photoelectron Spectroscopy (XPS), and Brunauer–Emmett–Teller (BET). Until now, to the best of our knowledge, there have been no reports published on the light-assisted synthesis of O-arylation of 2-chloroquinoline-3-carbaldehyde. Therefore, we explored the photocatalytic activity of the fabricated nanocomposite in the production of the O-arylated 2-chloroquinoline-3-carbaldehyde. This facile technique uses a blue LED light source as a non-conventional source and operates under moderate conditions, resulting in useful O-arylated products. The experimental data shows the good recyclability of the catalyst for up to five cycles without a loss in catalytic activity, a simple operational protocol, easy recoverability of the catalyst, and good product yields (65–90%) within 12–24 h. Additionally, the preliminary mechanistic investigations are discussed. The results show that the phenoxy and quinoline-3-carbaldehyde radicals generated upon blue LED irradiation during the course of the reaction are responsible for C-O bond formation, which results in O-arylation. The present study clearly indicates that 0D/2D nanocomposites have a bright future as metal-free, heterogeneous photocatalysts suitable for organic reactions.

Keywords: blue LED; O-arylation; photocatalyst; carbon nanodots; CDs/g-C₃N₄ heterojunction



Citation: Manjupriya, R.; Roopan, S.M. Unveiling the Photocatalytic Activity of Carbon Dots/g-C₃N₄ Nanocomposite for the O-Arylation of 2-Chloroquinoline-3-carbaldehydes. *Catalysts* **2023**, *13*, 308.
<https://doi.org/10.3390/catal13020308>

Academic Editor: Bo Hou

Received: 29 December 2022

Revised: 13 January 2023

Accepted: 28 January 2023

Published: 30 January 2023



Copyright: © 2023 by the authors. Licensee MDPI, Basel, Switzerland. This article is an open access article distributed under the terms and conditions of the Creative Commons Attribution (CC BY) license (<https://creativecommons.org/licenses/by/4.0/>).

1. Introduction

Aromatic ethers constitute one of the most basic organic molecular structures. As a result, various O-arylation processes for aromatic ether synthesis have been developed [1,2]. Ullmann coupling and Chan–Lam coupling are the most extensively used and most trustworthy technique of transition-metal-catalyzed O-arylation [3,4]. When transition metal poisoning from products is a concern, O-arylation by a metal-free catalyst is an appealing solution [5]. Because of its synthetic and response flexibility, as well as its wide range of chemical activity, 2-chloroquinoline-3-carbaldehyde chemistry has received a great deal of attention in recent years. These aldehydes are an intriguing class of organic compounds that could be used as synthetic intermediates and building blocks in the development of a wide range of heterocyclic systems, as well as presenting effective antibiotics for microbial and cancer therapy [6]. Furthermore, the quinoline molecule serves as the basic skeleton for many alkaloids found in nature, as well as anticancer treatments [7].

Catalysis is essential for chemical transformations and is fundamental to a vast array of chemical processes [8,9], ranging from academic laboratory research to industrial chemical applications. By employing catalytic reagents, it is possible to control the temperature during synthesis, reduce reagent waste, and enhance reaction selectivity, thereby potentially preventing unwanted side reactions and contributing to the development of green technology [10]. Nano-catalysis is widely used to speed up modern synthesis [11,12]. Typically, these catalysts are composed of nano-dimensional active constituents, distributed on a solid support. Achieving sustainability is the fundamental principle underlying the use of catalysts in organic synthesis [13,14]. Organic synthesis research in photocatalysis, particularly in relation to visible light, is also noteworthy [15,16].

Photochemistry is a branch of chemistry that studies chemical reactions caused by light absorption [17]. Photons are used in these chemical reactions to provide enough energy to convert the starting materials into the final products [18]. The most common visible light photocatalysts are expensive and hazardous polypyridyl complexes of ruthenium and iridium [19]. Furthermore, ligands are required for these species' catalytic activity, and tuning their chemical structures is critical to imparting the desired characteristics to metal-based photocatalysts [20]. Because of these considerations, there is currently a great deal of interest in developing novel, efficient, metal-free organic photocatalytic systems [21]. To meet these needs, these organic photocatalysts must be effective, safe, cheap, and easy to obtain using simple synthesis methods.

Photocatalysts based on graphitic carbon nitride ($g\text{-C}_3\text{N}_4$) are gaining popularity due to their unique electronic band structure and physicochemical properties [22,23]. With a bandgap of 2.7 eV, $g\text{-C}_3\text{N}_4$, shortly referred to as CN, is an environmentally friendly metal-free semiconductor [24,25]. Bonding with any metal, nonmetal, or doping agent with CN is necessary to improve its photocatalytic activities [26].

Carbon dots (CDs) have evolved as flexible metal-free substances with a wide range of features in terms of catalytic applications when it comes to metal-free catalysts [27,28]. Because of their inertness, high surface functionality, and chemical stability, CDs are an intriguing choice of support [29]. CDs are a fluorescent, potential group of zero-dimensional carbon nanomaterials composed of carbon cores (sp^2/sp^3 hybridized carbon), with sizes less than 10 nm, which are amorphous and poorly crystalline [30]. CDs have unique properties, such as outstanding water solubility at the nanoscale [31], strong photostability [32], and biocompatibility [33], in addition to captivating size- and excitation wavelength-dependent photoluminescence activity. All of these characteristics combine to make CDs environmentally friendly, safe, and cost-effective nanomaterials with a wide range of applications [34,35]. Similarly, the ease of their mass production from bioresources increases their versatility of applications [36]. In comparison with other carbon-based nanomaterials, such as carbon nanotubes [37] and graphene [38], the capability of CDs for catalytic processes in synthetic organic chemistry has yet to be fully revealed [39].

The optimum form of light source for photocatalytic applications is a light-emitting diode (LED). In terms of efficiency, energy, flexibility, longevity, and environmental friendliness, blue LEDs exceed other light sources. LEDs are an upgrade over traditional illumination sources due to their distinct properties; they provide designers with an additional conceptual scope while creating various photochemical reactions [40,41].

In 2017, Samanta and his colleagues [42] made a CDs/ Bi_2MoO_6 nanocomposite as a photocatalyst and tested its efficiency in the synthesis of benzimidazole. In 2017, Sarma et al. [43] used carbon nanodots with carboxyl groups on them to make several quinazolinones and aza-Michael adducts. In 2018, Majumdar et al. [44] came up with a new way to make quinazolinone derivatives from alcohol and 2-amino benzamide substrates in a single pot, using a CDs- Fe_3O_4 composite as a catalyst in an aqueous medium. Our research team has also recently published a review on carbon-dot-based organic transformations [45].

In terms of previous work, we report in this study for the first time on the photoirradiation of glucose-derived CDs/CN for promoting the O-arylation of 2-chloroquinoline-3-carbaldehydes. The Schottky-like heterojunction formed by the CDs/CN provides electron

mediation through the CDs, enhancing their photocatalytic activity. When compared to pristine CDs and CN, the prepared CDs/CN nanocomposite demonstrated higher photocatalytic activity and stability. UV-DRS, PL, FTIR, TEM, XRD, zeta potential, XPS, and BET were used to investigate the optical properties, functional group analysis, surface morphology, crystallinity, chemical stability, electronic properties, and pore size distribution of the samples. This study will pave the way for future advances in the field of photocatalysts in organic synthesis.

2. Results and Discussion

2.1. Characterization of the Prepared Nanocomposite

2.1.1. XRD Analysis

The XRD pattern revealed the crystalline nature and structure of the prepared materials. The XRD pattern of CN and various loading percentages of CD-modified CN nanocomposite are shown in Figure 1a. The pristine $g\text{-C}_3\text{N}_4$ has two strong peaks at about 13 and 27.3 degrees, which correspond to the (100) and (002) planes of graphitic carbon nitride (JCPDS No. 87-1526) [46]. No crystalline CDs were observed in the XRD patterns of the various as-fabricated loading percentages of CDs/ $g\text{-C}_3\text{N}_4$ nanocomposite (Figure 1a), which may be related to the low CD doping level. The primary diffraction peaks of the CN, however, are similar to the diffraction peaks of 3CDCN, 6CDCN, and 9CDCN. This demonstrates that the addition of CD did not alter or disrupt the structure of CN. Meanwhile, the major peaks of 3CDCN, 6CDCN, and 9CDCN shifted slightly, compared to CN, confirming that CDs were attached to the CN matrix.

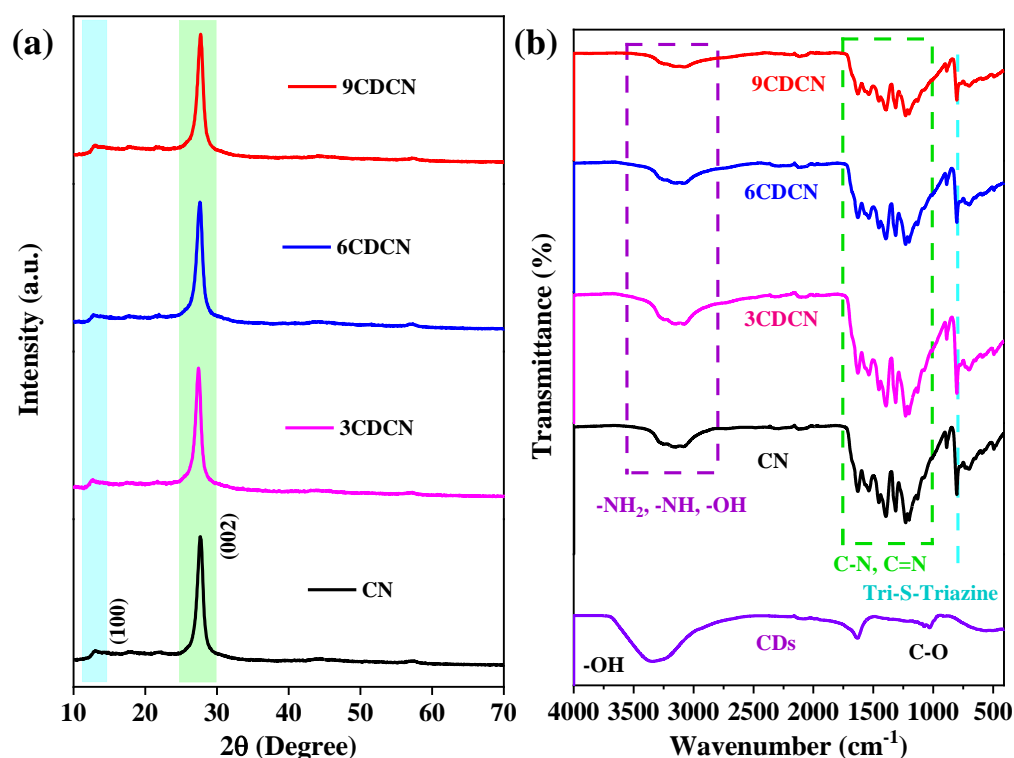


Figure 1. (a) The XRD pattern of CN, 3CDCN, 6CDCN, and 9CDCN, and (b) FT-IR spectrum of CDs, CN, 3CDCN, 6CDCN, and 9CDCN.

2.1.2. FT-IR Studies

Figure 1b depicts the functional groups of CN and the various CDs/CN nanocomposite materials. The broad peaks in the $3600\text{--}3000\text{ cm}^{-1}$ range are ascribed to the presence of -NH and -OH groups. The N-H stretching vibrational peaks in CN originate from the terminal -NH_2 or N-H groups, and O-H stretching or water molecule-absorbing peaks in CDs [47,48]. At 1750 cm^{-1} and 1250 cm^{-1} , respectively, vibrational absorption

bands corresponding to C=O and C-O-C were recorded on CDs [49]. The characteristic sharp peak at around 800 cm^{-1} corresponds to the triazine ring or vibration of the tri-s-triazine subunit [50]. As the percentage of CDs increases, the peaks shift slightly to the lower wavenumber side. The addition of CDs weakened the major characteristic peaks of CN in the FTIR spectrum of the CDs/CN nanocomposite, which was consistent with the XRD results.

2.1.3. XPS Studies

Surveys and elemental analysis are used in Figure 2a to further identify the amounts of C, N, and O. The results show that 3CDCN has a carbon/nitrogen mass ratio of 0.98, which is greater than that of CN (0.95), indicating that the carbon dots were successfully incorporated. In the XPS analysis of a 3CDCN nanocomposite, a trace amount of O (4.7%) is detected. The survey spectra in Figure 2a show that CN and 3CDCN contained only C, N, and O elements and no other impurities. The HR-XPS of C1s is shown in Figure 2b, where two distinct peaks at 288.1 and 285.0 eV are associated with carbon (sp^2 -hybridized) in the aromatic structure (N=C=N) and graphitic C-C, respectively, in CN [51,52].

A mixture of three peaks located at 287.1, 285.9, and 284.4 eV, which exhibit C atoms in the (N=C=N), C-O, and C-C, existing in the structure of 3CDCN (Figure 2b), can fit the C 1s XPS signal [53]. The HR-XPS N 1s spectra of CN (401.3, 399.8, 398.5 eV) and 3CDCN (400.3, 398.7, 397.5 eV) show several N species that can be attributed to amino functions (-NH), tertiary N bonded to carbon atoms (N-(C)3), and sp^2 -hybridized aromatic N (C=N-C) [54,55].

Meanwhile, the C1s and N1s orbital binding energies (CN) in the 3CDCN sample had shifted (Figure 2b,c). The results clearly show that when CN and CDs are combined, they form a heterojunction photocatalytic system with the highest electron density, and localize this charge in the C and N atoms [56].

2.1.4. TEM: Morphological Aspects

Figure 3 shows how the different HR-TEM magnifications and representative HR-TEM images were used to study the 3CDCN photocatalyst's characteristic shape and CD distribution. Figure 3a-c shows TEM images of the CN, CDs, and 3CDCN. The wrinkled 2D lamellar structure of the CN nanosheets with exfoliated layers can be seen in Figure 3a. The TEM images of the synthesized CDs are shown in Figure 3b. As can be seen, partial ethanol combustion produces relatively monodisperse CDs, with average sizes of 10 nm (Figure S1a in the Supplementary Materials). Figure 3c,e shows good CDs dispersion on CN nanosheets. The CDs in CN had an average size of 9.3 nm (Figure S1b in the Supplementary Materials), which was slightly smaller than pristine CDs. The HR-TEM images (Figure 3d) show that CDs have crystalline nature, with a lattice spacing of around 0.31 nm (Figure S1c in the Supplementary Materials). Furthermore, highly dispersed CDs are clearly visible (Figure 3f), implying that CDs were successfully incorporated into CN and formed a heterojunction.

2.1.5. BET Surface Area

Surface area is a key metric that influences photocatalytic activity because the process is surface-dependent. The active sites are bigger and have stronger photocatalytic activity when the surface area is larger [57]. The BET-specific surface area of 3CDCN is observed by the N_2 adsorption and desorption isotherms, as shown in Figure 4a. The BET-specific surface area of 3CDCN ($108.532\text{ m}^2/\text{g}$) is significantly greater than that of CN [58], indicating that the CDs are attached to the surface of CN nanosheets. A larger BET surface area generates more active sites, which is beneficial for substrate adsorption and photocatalytic performance.

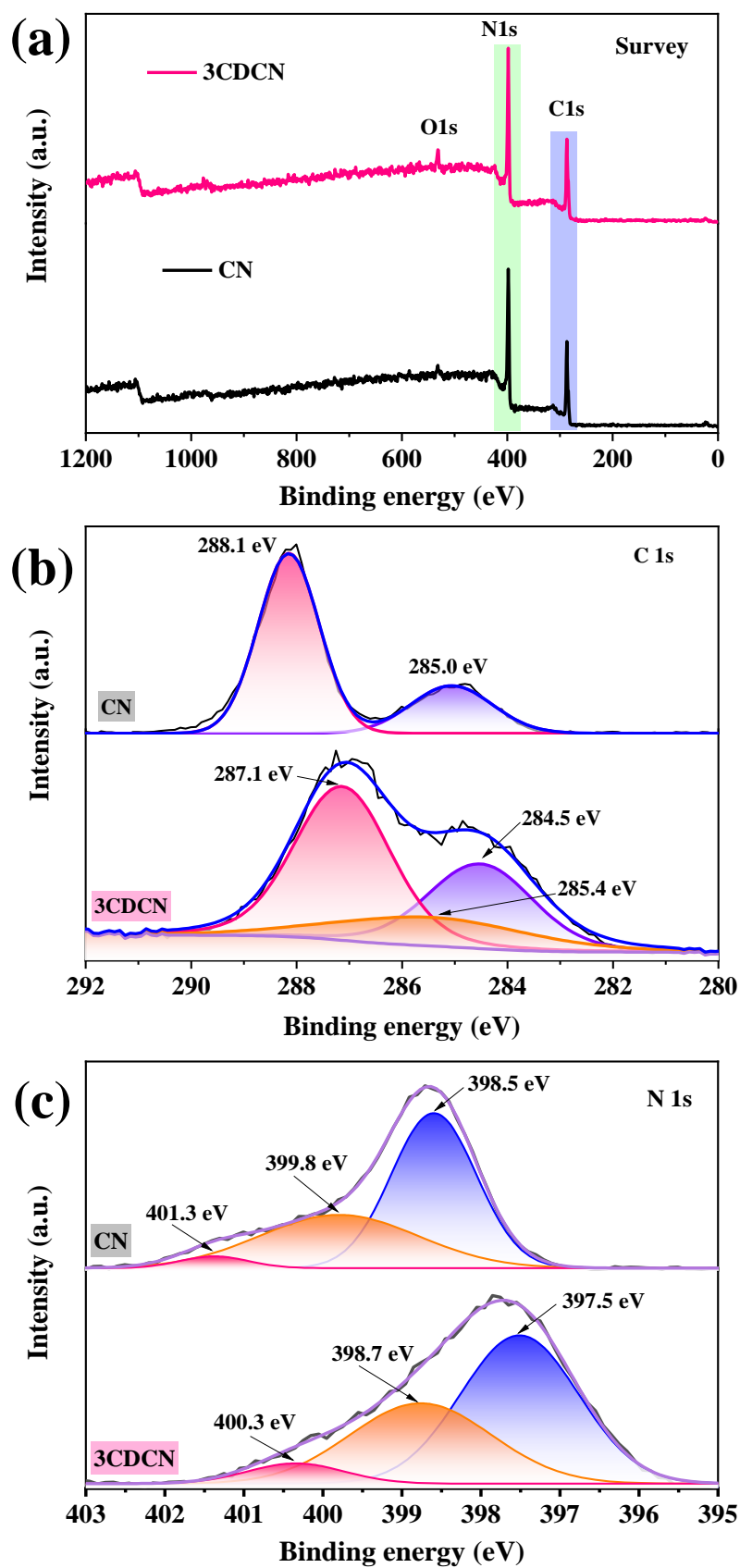


Figure 2. XPS spectra of CN and 3CDCN (a) survey spectra, (b) the HR-XPS of carbon, and (c) the HR-XPS of nitrogen.

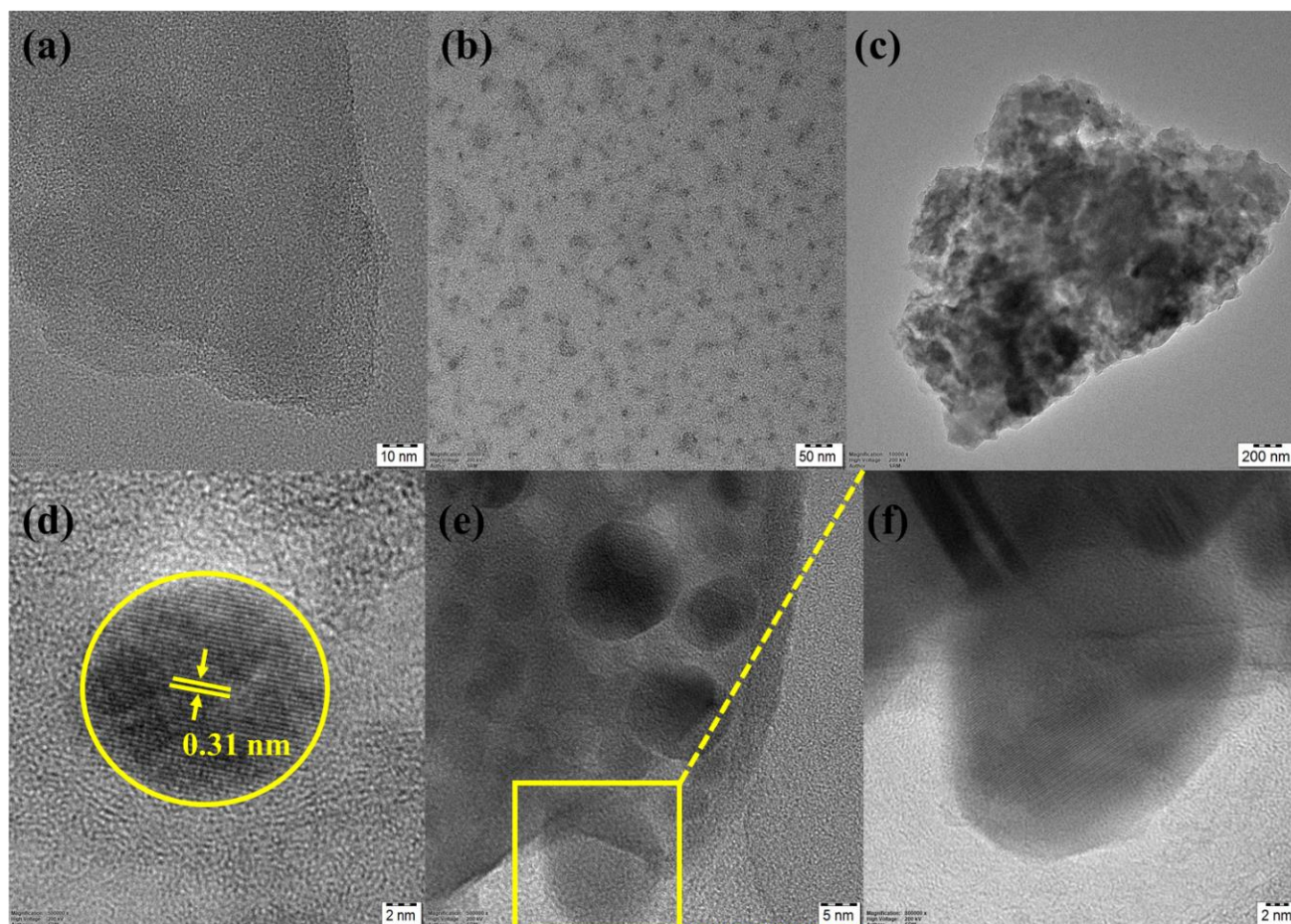


Figure 3. TEM images of (a) CN, (b) CDs, (c) 3CDCN, HR-TEM of (d) CDs, (e) 3CDCN at a 5 nm scale, and (f) 3CDCN at a 2 nm scale.

2.1.6. Zeta Surface Charge Potential

The zeta potential value of the pristine CN and CD-loaded nanocomposites was measured, and the results are shown in Figure 4b. CN nanosheets have a zeta potential value of -21.9 mV, indicating that their surface is negatively charged, whereas the zeta potential value of pristine CDs was found to be 20.3 mV. CDs loaded with 3CDCN, 6CDCN, and 9CDCN have zeta potentials of 13.9 mV, 25.6 mV, and 24.1 mV, respectively. This means that the CDs were successfully designed on CN surfaces. Electrostatic attraction aids in the formation of uniform distribution and deposits CDs in the 3CDCN nanocomposite.

2.1.7. Thermal Stability of 3CDCN

The thermal stability of the nanocomposite was characterized by the TGA and DTA curves. The initial decomposition of CN was recorded at 400 °C and the complete weight loss was observed at 720 °C, which is due to the combustion of carbon, while for 3CDCN, it started to decompose earlier at 300 °C than CN, and complete decomposition occurred as with CN. This clearly indicates the incorporation of CDs into CN. The experimental findings revealed that 3CDCN was thermally stable up to 600 °C (Figure 4c).

2.1.8. Optical Properties

Changes in the UV-vis absorption spectra could be used to detect surface functionality variations. As a result, Figure 5a depicts the UV-vis spectra of glucose and as-synthesized CDs, emphasizing the distinct influence of reaction time. Finally, 30 min of microwave irradiation resulted in the formation of a new absorbance peak at 280 nm, with non-bonding orbitals such as C=O bonds attributed to the $n \rightarrow \pi^*$ transitions. The optical properties were

analyzed using UV-vis DRS spectra (Figure 5c), and the relevant band gap was estimated using Tauc's plot (Figure 5c). At about 470 nm, pure $g\text{-C}_3\text{N}_4$ exhibited a fundamental absorption edge. As the number of CDs that were being loaded increased, the absorption edge in red gradually migrated from the beginning at 470 nm. This finding implies that when CN is hybridized with CDCN, it can harvest more visible light, which is crucial for improving photocatalytic performance because better visible light utilization can result in producing more effective photo-generated electron-hole pairs. The band gap of pure CN was calculated to be approximately 2.77 eV, which is very similar to previous $g\text{-C}_3\text{N}_4$ results [59]. The band gaps of 3CDCN, 6CDCN, and 9CDCN were 2.4, 2.2, and 1.9 eV, respectively, indicating that they narrowed progressively from 2.4 to 1.9 eV when increasing the loading of CDs.

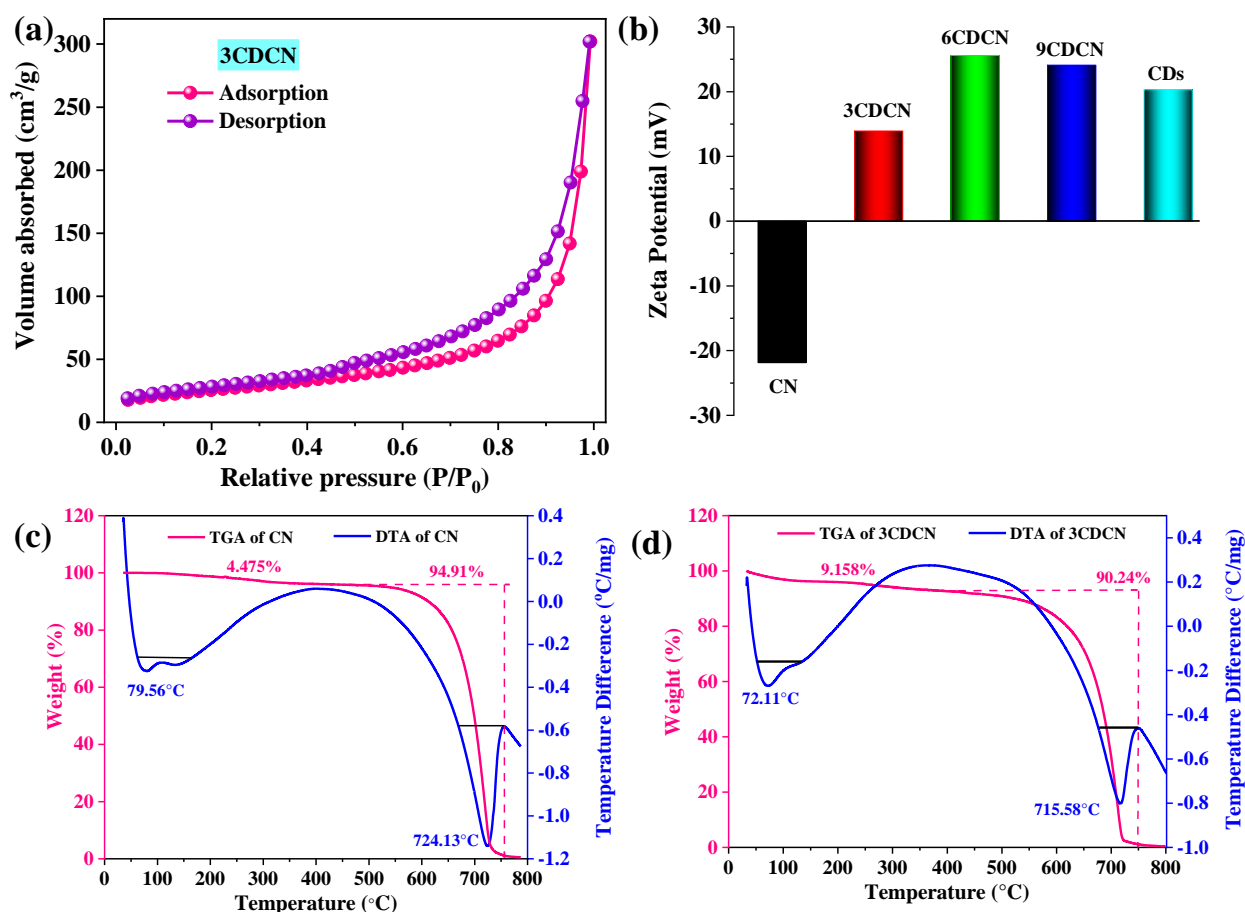


Figure 4. (a) BET isotherm of the 3CDCN nanocomposite, (b) Zeta potential of CN, 3CDCN, 6CDCN and 9CDCN, CDs and TGA, and the DTA graph of (c) CN and (d) 3CDCN.

The photogenerated charge carrier separation efficiency in semiconductors is frequently investigated, using PL emission spectroscopy [60]. The PL emission signal is produced by the combination of excited electrons and holes. Figure 5d depicts the PL emission spectra of the as-prepared photocatalysts, stimulated at 390 nm. A broad emission peak with a center wavelength of about 458 nm, as seen in all CDCN photocatalysts, could be attributed to the band–band PL phenomenon of the photo-induced charge carriers for CN. The 3CDCN, 6CDCN, and 9CDCN composites exhibited significant PL quenching when compared to the CN, due to the effective charge transfer at the heterostructure interface [61].

2.2. Photocatalytic Activity of CDs/g-C₃N₄ in the O-Arylation of 2-Chloroquinoline-3-carbaldehyde

After all the characterizations of CDCN were performed, the photocatalytic application of CDCN was incorporated into the O-arylation of quinoline-3-carbaldehyde. The reaction of 2-chloroquinoline-3-carbaldehyde (1) and 4-bromophenol (2) was chosen as a model reaction (Scheme 1). Initially, reaction parameters such as catalyst, base, solvent, and light parameters were optimized. Various carbon materials were used in the catalyst selection process. All the chosen materials demonstrated a significant yield. However, 3CDCN was shown to have a higher yield in terms of efficiency and catalyst separation. When the loading weight percentage of 3CDCN was examined, it was shown that 10 wt % (9.6 mg) catalysts loading produced the highest yield (Table 1). When the loading weight percentage of 3CDCN exceeds 10 wt %, there is no change in the yield of the product and turbidity also occurs in the reaction. Turbidity affects the yield of the reaction by screening the interaction between the light source and the reactants in the reaction mixture. Therefore, we fixed the optimized catalyst loading as 10 wt %. Therefore, further reaction parameters were optimized with the use of a 10 wt % catalyst.

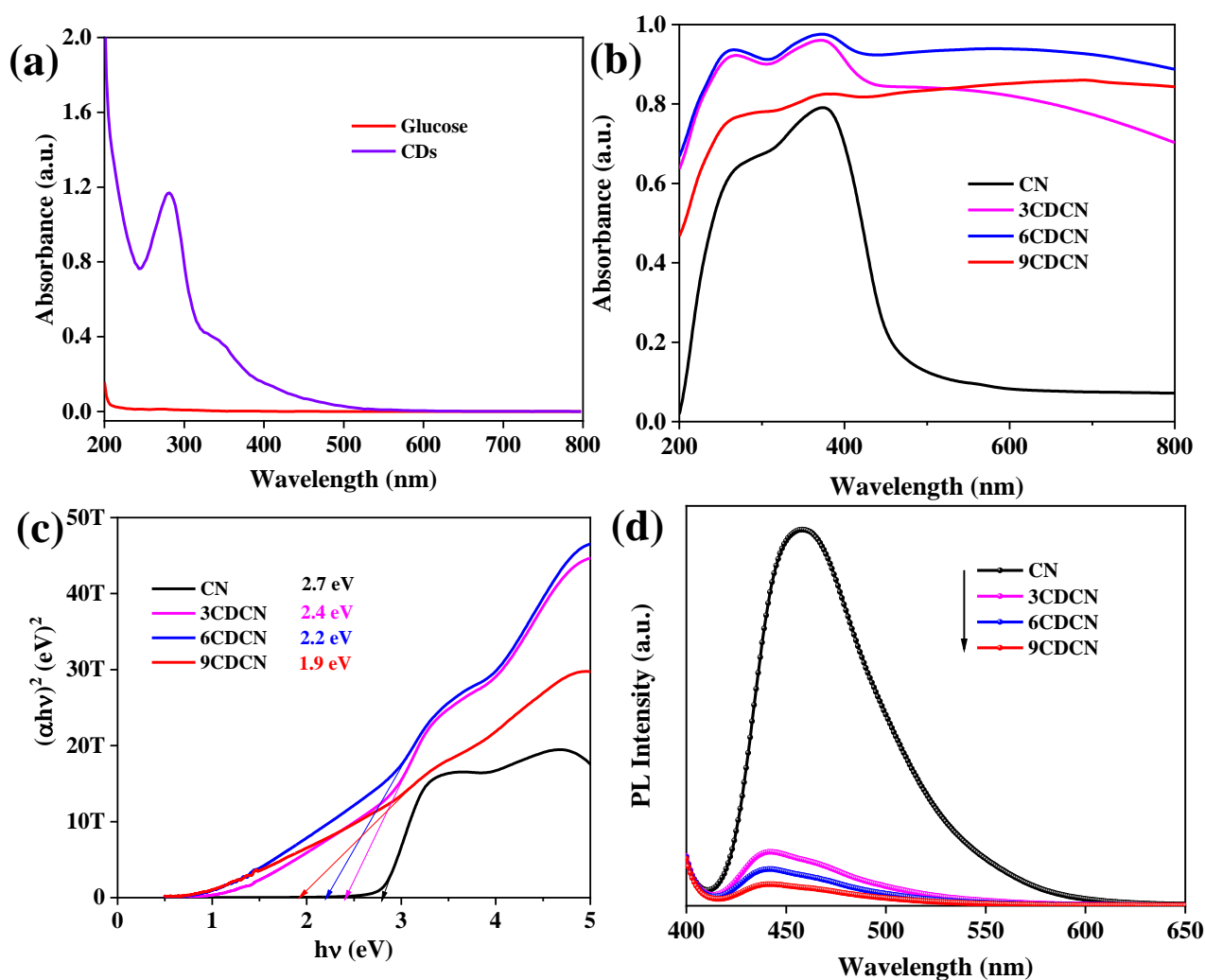


Figure 5. (a) UV absorption spectra of glucose and CDs. Prepared nanomaterials: CN, 3CDCN, 6CDCN, and 9CDCN. (b) UV-vis DRS spectra, (c) band gap, and (d) PL spectra.

In terms of base optimization, the reaction was initially carried out in DMF without the use of a base. The reaction condition did not produce the desired product. This is due to the importance of the base in proton abstraction. Furthermore, the reaction conditions were tuned using weak bases, such as Na_2CO_3 and K_2CO_3 , and strong bases, such as NaOH and KOH. All the bases that were chosen demonstrated a prominent yield. Mild bases were used to produce a significant yield, particularly K_2CO_3 (Table 2). Therefore, solvent and light optimization was carried out in the presence of K_2CO_3 as a base. Non-polar, polar protic, and aprotic solvents were used to investigate the effect of solvent on the O-arylation of quinolines. It has been observed that non-polar solvents, such as hexane, tend to suppress the reaction. The effect of the solvent was further investigated by experimenting with polar protic and aprotic solvents.

Table 2. Optimization of the base.

S. No.	Base	Catalyst	Solvent Medium	Yield ^a (%)
1.	-	3CDCN	DMF	<5%
2.	K_2CO_3	3CDCN	DMF	90%
3.	Na_2CO_3	3CDCN	DMF	59%
4.	KOH	3CDCN	DMF	55%
5.	t-BuOK	3CDCN	DMF	35%

Conditions: 2-chloroquinoline-3-carbaldehyde (0.5 mmol, 96 mg, 1 equiv.), 4-bromophenol (0.5 mmol, 86 mg, 1 equiv.), Base (1 mmol, 138 mg, 2 equiv.), DMF (2 mL), 3CDCN (9.6 mg, 10 wt %), blue LED (12 W, 450–495 nm), time 12 h, ambient temperature, ^a isolated yields.

The reaction did not proceed well and did not give the desired product with the use of polar protic solvents (EtOH and MeOH). The formation of by-products was observed. The reaction went smoothly and produced the desired product when polar aprotic solvents (DMF, DMSO, and ACN) were used. Reactions with H_2O as a reaction medium failed to initiate the conversion of the product. However, DMF tended to have a better yield (Table 3).

Table 3. Optimization of Solvent.

S. No.	Solvent Medium	Base	Catalyst	Yield ^a (%)
1.	EtOH	K_2CO_3	3CDCN	NR
2.	MeOH	K_2CO_3	3CDCN	NR
3.	H_2O	K_2CO_3	3CDCN	NR
4.	Hexane	K_2CO_3	3CDCN	NR
5.	THF	K_2CO_3	3CDCN	Trace
6.	ACN	K_2CO_3	3CDCN	41%
7.	DMSO	K_2CO_3	3CDCN	82%
8.	DMF/ H_2O	K_2CO_3	3CDCN	20%
9.	DMF	K_2CO_3	3CDCN	90%

Conditions: 2-chloroquinoline-3-carbaldehyde (0.5 mmol, 96 mg, 1 equiv.), 4-bromophenol (0.5 mmol, 86 mg, 1 equiv.), K_2CO_3 (1 mmol, 138 mg, 2 equiv.), solvent (2 mL), 3CDCN (9.6 mg, 10 wt %), blue LED (12 W, 450–495 nm), time 12 h, ambient temperature, ^a isolated yields.

To generate UV or visible light, classical photocatalysis depends mostly on xenon or high-pressure mercury lamps. Although this provides a consistent light source, it consumes a great deal of energy and generates a large amount of heat. As a result, in recent years, LED light sources have attracted attention in terms of photocatalysis, due to their low-energy, practical, and dependable qualities. Table 4 discusses the optimization of visible light of different powers (150, 300, and 500 W) and blue LED (12 W, 450–495 nm). Reactions carried

out under visible light had a prominent yield (42–69%), while reactions with blue LED gave a higher yield of 90%. This is because the photocatalyst under study had a band edge in the region of 400–500 nm; this is in accordance with the UV-vis DRS plot (Figure 5b). Thus, the photocatalyst could absorb light effectively between 400 and 500 nm. Out of the diverse lights considered in this study, the blue LED showed better photocatalytic activity in terms of lower energy consumption and allows the photocatalyst to absorb light in this spectral region. With the light-optimized conditions in hand (Table 4), the scope of the diverse substrates was carried out. Unsubstituted phenol gave the corresponding O-arylation product (3.1), with an 88% yield. The reactions of phenols containing halogens, such as 4-Br (3.2) and 4-Cl (3.3), proceeded well, with high to excellent yields (87–90%). However, the reactions of phenol with electron-withdrawing substituents, such as 4-NO₂ (3.4), gave a moderate yield of 65%. The reactions of phenols with electron-donating groups similar to 4-OMe (3.5) proceeded substantially well, giving good yields (83%). Furthermore, an aliphatic alcohol substrate yielded the corresponding ether (3.7) at an 89% yield. Furthermore, we strove to examine the catalyst potential of unusual alcohols instead of the substituted phenols (Scheme 1).

Table 4. Optimization of the light source.

S. No.	Catalyst	Base	Solvent Medium	Condition	Yield ^a (%)
1.	3CDCN	K ₂ CO ₃	DMF	Visible light (150 W)	42%
2.	3CDCN	K ₂ CO ₃	DMF	Visible light (300 W)	69%
3.	3CDCN	K ₂ CO ₃	DMF	Visible light (500 W)	55%
4.	3CDCN	K ₂ CO ₃	DMF	Blue LED (12 W, 450–495 nm)	90%

Note: 2-chloroquinoline-3-carbaldehyde (0.5 mmol, 96 mg, 1 equiv.), 4-bromophenol (0.5 mmol, 86 mg, 1 equiv.), K₂CO₃ (1 mmol, 138 mg, 2 equiv.), DMF (2 mL), 3CDCN (9.6 mg, 10 wt %), light source, time 12 h, ambient temperature, ^a isolated yields.

The formation of the product was confirmed by ¹H NMR, ¹³C NMR, GCMS, HRMS, and FTIR analyses (Figures S2–S30 in the Supplementary Materials). The formation of compound 3.6 was identified by ¹H NMR, ¹³C NMR, HR-MS, and FTIR. The signal for the -OH proton in ¹H NMR vanished around 9–10 ppm, confirming the formation of the C-O bond between quinoline and the alcohol moiety. Further, by comparing the FTIR plots of the reactant (alcohol moiety) and the product, 3.6, we can see that the disappearance of the -OH stretching (3404 cm⁻¹) in the product, 3.6, strongly indicates the O-arylation of quinoline with the alcohol moiety. Moreover, HR-MS revealed the molecular mass of the predicted compound.

2.2.1. Plausible Mechanism

Relying on all these findings, we propose a plausible mechanism, as illustrated in Figure 6. Under light irradiation, the 3CDCN nanocomposite absorbs light, resulting in photoinduced electron-hole pairs in the conduction and valence bands. The produced charge carriers are then counterbalanced by recombination, when a few of them move to the composite's surface [62]. Thus, the photocatalyst becomes excited. Then, the excited electrons in the conduction band can easily flow through CDs. Thus, a Schottky-like heterojunction is formed [63]. This excited photocatalyst thus induces the homolytic C-Cl bond cleavage of 1, producing 1a. This radical generation is induced by the single-electron transfer (SET) of the photoexcited catalyst, where the photoreduction takes place [64]. Accordingly, the intermediate, 2a, is found to be produced by the proton abstraction of 2 by

the base. Then, photo-oxidation takes place, thus generating the phenoxy radical, **2b** [65]. Finally, the radical-generated moieties, **1b** and **2b**, couple together to produce the desired O-arylated product, **3**, by the elimination of KCl.

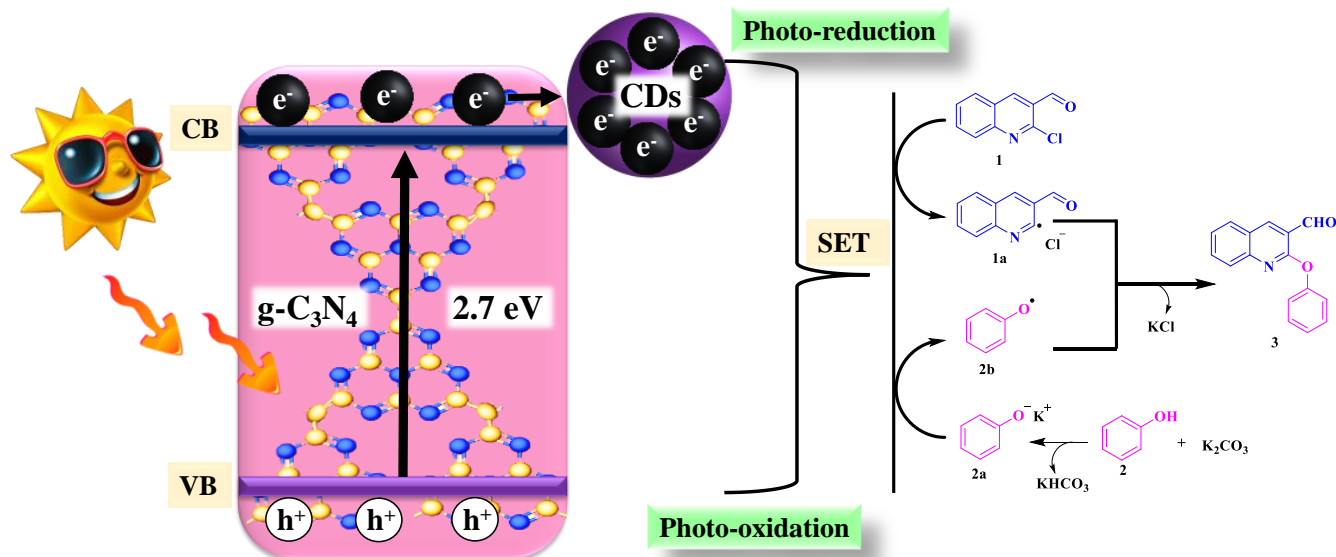


Figure 6. The charge transfer mechanism of the CDCN nanocomposite and a plausible mechanism.

2.2.2. Radical Scavenging Study

The identified suppression of the reaction in an oxygen atmosphere was congruent with the proposed radical mechanism. This was further supported by a study performed in the presence of a free radical scavenger, 2,2,6,6-tetramethylpiperidine-1-oxyl (TEMPO, 1 equiv). As expected, the desired product, **3**, has not been detected. This proves the generation of radicals during the course of the reaction.

2.2.3. Reusability and Stability Tests

Figure 7 depicts the 3CDCN photocatalyst recovery and reuse activities. In the current study, 3CDCN was collected by centrifugation, washed with acetone, and reused in the subsequent round of photocatalytic reactions. According to Figure 7a, the photocatalytic performance slightly declined after four trials, to 80%. This small decline in 3CDCN photocatalytic activity could be due to the material losses that might occur during the recovery process (washing and drying), which would result in a reduced dose in the following cycle, hence reducing the specific surface catalytic activity and lowering the performance. In order to determine the reason for this decrease in the photocatalytic performance of 3CDCN during its recycling, in terms of the photocatalytic O-arylation of 2-chloroquinoline-3-carbaldehydes, the physicochemical properties of the fresh and recycled 3CDCN nanocomposite were compared via XRD and XPS analyses. After the process was completed, the 3CDCN photocatalyst's XRD patterns and XPS (C1s and N1s) findings remained consistent, demonstrating that no significant structural or chemical changes occurred in the 3CDCN photocatalyst (Figure 7b,d). Thus, it can be said that the CDs/g-C₃N₄ nanocomposite photocatalyst was stable and had the potential to be used in industrial applications.

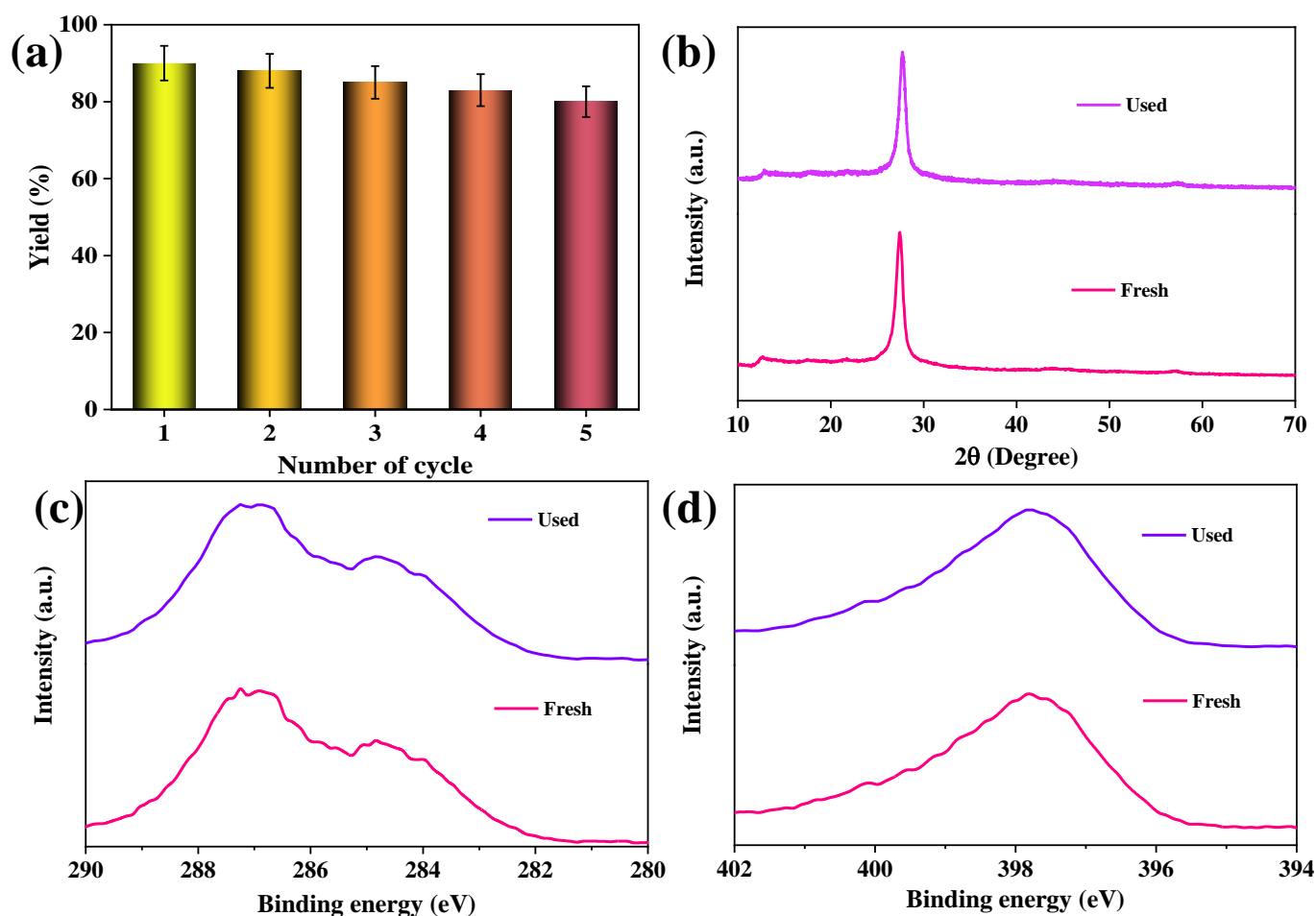


Figure 7. (a) Reusability of the 3CDCN photocatalyst and the stability of fresh and used 3CDCN, (b) XRD pattern, (c) XPS of C1s, and (d) XPS of N1s.

3. Materials and Methods

3.1. Details of the Materials Used

The details are available in the supporting document (Text S1).

3.2. Microwave-Assisted Synthesis of Carbon Dots

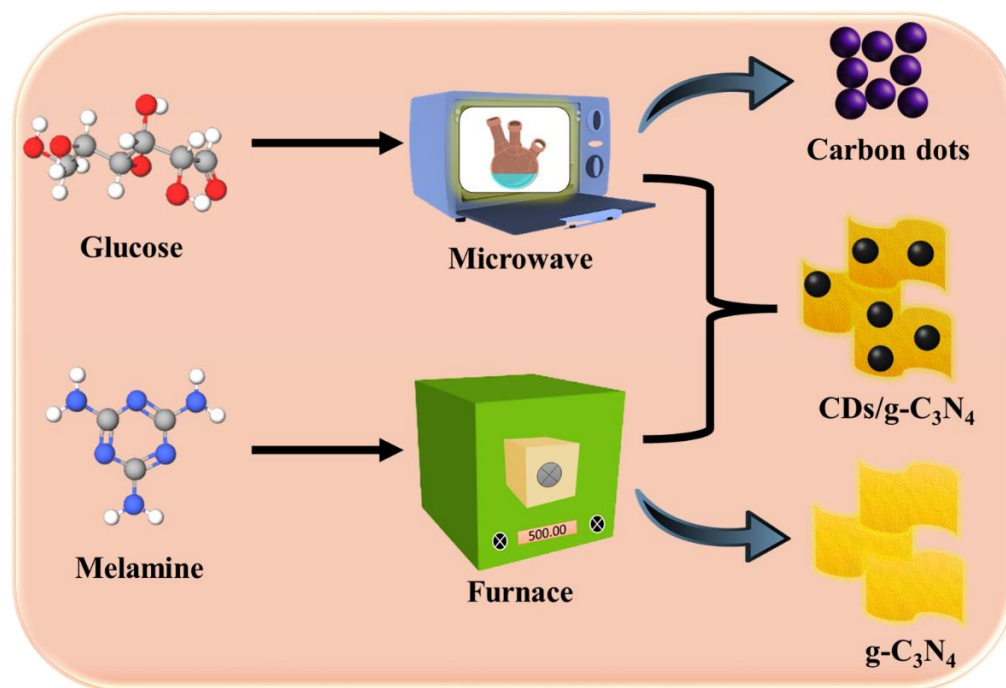
The CDs were made from glucose in a single step using a microwave. In a beaker, 3 g of glucose was dissolved in 10 mL of deionized water. Then, 6 mL of concentrated HCl solution was gradually added to the glucose solution. The mixture was then poured into a three-neck microwave vial for microwave heating (90 °C). The entire mixture was placed in a microwave oven with 500 watts of power for 30 min. As the CDs formed, the color of the mixture changed from colorless to dark brown. Before dialysis, the brown solution was centrifuged at 8000 rpm for 30 min and then filtered through a 0.22 μm membrane after naturally cooling to room temperature. Finally, the obtained CDs were dialyzed for 10 h against ultra-pure water and were stored at 3 °C in the refrigerator before being used in the subsequent experiments.

3.3. Preparation of g-C₃N₄ Nanosheets

First, 10 g of melamine was calcined at 550 °C in a muffle furnace for 3 h (10 °C min⁻¹). The bulk g-C₃N₄ sample was then ground into powder and exfoliated using ultrasonication, similar to the procedure described previously in the literature [58].

3.4. Fabrication of CDs/g-C₃N₄ Composite

Scheme 2 depicts an overall composite preparation schematic and representation diagram. Under constant stirring, 1 g of g-C₃N₄ nanosheets was dispersed in 10 mL of deionized water. The g-C₃N₄ suspension was then treated with microwave-assisted synthesized CD solutions of varying concentrations (300, 600, and 900 µL). Finally, the mixture was subjected to a piezoelectric process for 30 min before being heated at 180 °C for 2 h. CD concentrations of 300, 600, and 900 µL were labeled as 3CDCN, 6CDCN, and 9CDCN, respectively.



Scheme 2. The schematic synthesis procedure of the CDs/g-C₃N₄ nanocomposite.

3.5. Characterization Details

The details are available in the supporting document (Text S2).

3.6. General Procedure for the Synthesis of O-Arylated 2-Chloroquinoline-3-carbaldehydes (3)

The compound (**1**) was prepared and compared with the method in the literature [66]. Yield 79%, m.p. 148 °C. For the O-arylation of 2-chloroquinoline-3-carbaldehydes, the reaction vial was charged with 2-chloroquinoline-3-carbaldehyde (0.5 mmol, 96 mg, 1 equiv.), substituted phenol (0.5 mmol, 1 equiv.), K₂CO₃ (2 mmol, 138 mg, 2 equiv.), DMF (2 mL), and photocatalyst (9.6 mg, 10 wt %). The mixture was irradiated under blue LED (12W, 495 nm) for 12–24 h until the product was formed. The reaction was monitored by TLC. After completion of the reaction, the reaction mixture was poured into crushed ice, filtered, dried, and column-purified, using ethyl acetate/petroleum ether (1:9) as an eluent.

4. Conclusions

In summary, we prepared a facile CDs/g-C₃N₄ heterojunction and explored its optical properties, surface morphology, surface functionality, crystallinity, chemical stability, electronic properties, and pore-size distribution through various characterization techniques. The constructed photocatalyst has been explored for its photocatalytic activity in the successful O-arylation of 2-chloro-3-formyl quinolines. The efficiency of the catalyst could be extended to diverse substrates. Based on the research findings, 10 wt % of CDs/g-C₃N₄ nanocomposite exhibited the best photocatalytic activity when compared to pristine CDs and g-C₃N₄. The reaction has been carried out with the irradiation of

low energy-consumption blue LEDs. The catalyst that was taken into account exhibited excellent recyclability, easy recoverability, and good reusability. We hope that this will spark a wave of investigation and open up a theme that we anticipate will emerge as one of the most prevalent concepts in the coming years.

Supplementary Materials: The following supporting information can be downloaded at: <https://www.mdpi.com/article/10.3390/catal13020308/s1>, Figure S1: Particle size histogram of (a) CDs, (b) 3CDCN, and (c) HRTEM d-spacing value of 3CDCN calculation; Figures S2–S30: FT-IR, ^1H , ^{13}C NMR and HR-MS spectra of substituted quinoline-3-carbaldehydes 3.1–3.7. Text S1: Materials details. Text S2: Characterization details.

Author Contributions: Investigation, data curation, and original draft preparation, R.M.; conceptualization, formal analysis, writing—review and editing, and supervision, S.M.R. All authors discussed the results and contributed to the final manuscript. All authors have read and agreed to the published version of the manuscript.

Funding: This research received no external funding.

Data Availability Statement: Not applicable.

Acknowledgments: Our profound thanks go to the management of the Vellore Institute of Technology for providing a Sophisticated Instrument Facility (SIF) and for the fellowship offered to Manjupriya to aid in the research endeavor.

Conflicts of Interest: The authors declared no potential conflict of interest.

References

1. Theil, F. Synthesis of Diaryl Ethers: A Long-Standing Problem Has Been Solved. *Angew. Chemie Int. Ed.* **1999**, *38*, 2345–2347. [[CrossRef](#)]
2. Zhang, H.; Chen, L.; Oderinde, M.S.; Edwards, J.T.; Kawamata, Y.; Baran, P.S. Chemoselective, Scalable Nickel-Electrocatalytic O-Arylation of Alcohols. *Angew. Chem.* **2021**, *133*, 20868–20873. [[CrossRef](#)]
3. Grushin, V.V.; Alper, H. Transformations of Chloroarenes, Catalyzed by Transition-Metal Complexes. *Chem. Rev.* **1994**, *94*, 1047–1062. [[CrossRef](#)]
4. Collman, J.P.; Zhong, M. An Efficient Diamine-Copper Complex-Catalyzed Coupling of Arylboronic Acids with Imidazoles. *Org. Lett.* **2000**, *2*, 1233–1236. [[CrossRef](#)] [[PubMed](#)]
5. Zhao, J.; Zhao, Y.; Fu, H. Transition-Metal-Free Intramolecular Ullmann-Type O-Arylation: Synthesis of Chromone Derivatives. *Angew. Chem. Int. Ed.* **2011**, *50*, 3769–3773. [[CrossRef](#)]
6. Sangu, K.; Fuchibe, K.; Akiyama, T. A Novel Approach to 2-Arylated Quinolines: Electrocyclization of Alkynyl Imines via Vinylidene Complexes. *Org. Lett.* **2004**, *6*, 353–355. [[CrossRef](#)]
7. Rajakumar, P.; Raja, R.; Selvam, S.; Rengasamy, R.; Nagaraj, S. Synthesis and Antibacterial Activity of Some Novel Imidazole-Based Dicationic Quinolnophanes. *Bioorg. Med. Chem. Lett.* **2009**, *19*, 3466–3470. [[CrossRef](#)]
8. Radini, I.; Elsheikh, T.; El-Telbani, E.; Khidre, R. New Potential Antimalarial Agents: Design, Synthesis and Biological Evaluation of Some Novel Quinoline Derivatives as Antimalarial Agents. *Molecules* **2016**, *21*, 909. [[CrossRef](#)]
9. Chellapandi, T.; Madhumitha, G. Montmorillonite Clay-Based Heterogenous Catalyst for the Synthesis of Nitrogen Heterocycle Organic Moieties: A Review. *Mol. Divers.* **2021**, *26*, 2311–2339. [[CrossRef](#)]
10. Shiri, L.; Ghorbani-Choghamarani, A.; Kazemi, M. S-S Bond Formation: Nanocatalysts in the Oxidative Coupling of Thiols. *Aust. J. Chem.* **2017**, *70*, 9. [[CrossRef](#)]
11. Xu, H.-J.; Wan, X.; Geng, Y.; Xu, X.-L. The Catalytic Application of Recoverable Magnetic Nanoparticles-Supported Organic Compounds. *Curr. Org. Chem.* **2013**, *17*, 1034–1050. [[CrossRef](#)]
12. Niakan, M.; Masteri-Farahani, M.; Shekaari, H.; Karimi, S. Pd Supported on Clicked Cellulose-Modified Magnetite-Graphene Oxide Nanocomposite for C-C Coupling Reactions in Deep Eutectic Solvent. *Carbohydr. Polym.* **2021**, *251*, 117109. [[CrossRef](#)] [[PubMed](#)]
13. Dhakshinamoorthy, A.; Garcia, H. Catalysis by Metal Nanoparticles Embedded on Metal-Organic Frameworks. *Chem. Soc. Rev.* **2012**, *41*, 5262. [[CrossRef](#)] [[PubMed](#)]
14. Nagarjun, N.; Jacob, M.; Varalakshmi, P.; Dhakshinamoorthy, A. UiO-66(Ce) Metal-Organic Framework as a Highly Active and Selective Catalyst for the Aerobic Oxidation of Benzyl Amines. *Mol. Catal.* **2021**, *499*, 111277. [[CrossRef](#)]
15. König, B. Photocatalysis in Organic Synthesis—Past, Present and Future. *Eur. J. Org. Chem.* **2017**, *2017*, 1979–1981. [[CrossRef](#)]
16. Arunachalapani, M.; Roopan, S.M. Visible Light-Activated Cu_3TiO_4 Photocatalyst for the One-Pot Multicomponent Synthesis of Imidazo-Pyrimido Acridines. *Inorg. Chem. Commun.* **2023**, *148*, 110310. [[CrossRef](#)]
17. Gisbertz, S.; Pieber, B. Heterogeneous Photocatalysis in Organic Synthesis. *ChemPhotoChem* **2020**, *4*, 456–475. [[CrossRef](#)]
18. Romero, N.A.; Nicewicz, D.A. Organic Photoredox Catalysis. *Chem. Rev.* **2016**, *116*, 10075–10166. [[CrossRef](#)]

19. Dutta, S.; Erchinger, J.E.; Schäfers, F.; Das, A.; Daniliuc, C.G.; Glorius, F. Chromium/Photoredox Dual Catalyzed Synthesis of α -Benzylic Alcohols, Isochromanones, 1,2-Oxy Alcohols and 1,2-Thio Alcohols. *Angew. Chem. Int. Ed.* **2022**, *61*, e202212136. [[CrossRef](#)]
20. Kundu, S.; Roy, L.; Maji, M.S. Development of Carbazole-Cored Organo-Photocatalyst for Visible Light-Driven Reductive Pinacol/Imino-Pinacol Coupling. *Org. Lett.* **2022**, *24*, 9001–9006. [[CrossRef](#)]
21. Bhuyan, S.; Gogoi, A.; Basumatary, J.; Gopal Roy, B. Visible-Light-Promoted Metal-Free Photocatalytic Direct Aromatic C–H Oxygenation. *Eur. J. Org. Chem.* **2022**, *16*, e202200148. [[CrossRef](#)]
22. Alaghmandfard, A.; Ghandi, K. A Comprehensive Review of Graphitic Carbon Nitride (g-C₃N₄)–Metal Oxide-Based Nanocomposites: Potential for Photocatalysis and Sensing. *Nanomaterials* **2022**, *12*, 294. [[CrossRef](#)] [[PubMed](#)]
23. Mun, S.J.; Park, S.-J. Graphitic Carbon Nitride Materials for Photocatalytic Hydrogen Production via Water Splitting: A Short Review. *Catalysts* **2019**, *9*, 805. [[CrossRef](#)]
24. Arunachalapandi, M.; Roopan, S.M. Environment Friendly G-C₃N₄-Based Catalysts and Their Recent Strategy in Organic Transformations. *High Energy Chem.* **2022**, *56*, 73–90. [[CrossRef](#)]
25. Wang, J.; Wang, S. A Critical Review on Graphitic Carbon Nitride (g-C₃N₄)-Based Materials: Preparation, Modification and Environmental Application. *Coord. Chem. Rev.* **2022**, *453*, 214338. [[CrossRef](#)]
26. Chen, J.; Fang, S.; Shen, Q.; Fan, J.; Li, Q.; Lv, K. Recent Advances of Doping and Surface Modifying Carbon Nitride with Characterization Techniques. *Catalysts* **2022**, *12*, 962. [[CrossRef](#)]
27. Arcudi, F.; Đorđević, L.; Prato, M. Design, Synthesis, and Functionalization Strategies of Tailored Carbon Nanodots. *Acc. Chem. Res.* **2019**, *52*, 2070–2079. [[CrossRef](#)]
28. Lim, S.Y.; Shen, W.; Gao, Z. Carbon Quantum Dots and Their Applications. *Chem. Soc. Rev.* **2015**, *44*, 362–381. [[CrossRef](#)]
29. Wang, Y.; Hu, A. Carbon Quantum Dots: Synthesis, Properties and Applications. *J. Mater. Chem. C* **2014**, *2*, 6921. [[CrossRef](#)]
30. Du, Y.; Guo, S. Chemically Doped Fluorescent Carbon and Graphene Quantum Dots for Bioimaging, Sensor, Catalytic and Photoelectronic Applications. *Nanoscale* **2016**, *8*, 2532–2543. [[CrossRef](#)]
31. Dey, D.; Bhattacharya, T.; Majumdar, B.; Mandani, S.; Sharma, B.; Sarma, T.K. Carbon Dot Reduced Palladium Nanoparticles as Active Catalysts for Carbon-Carbon Bond Formation. *Dalt. Trans.* **2013**, *42*, 13821. [[CrossRef](#)]
32. Zhi, B.; Gallagher, M.J.; Frank, B.P.; Lyons, T.Y.; Qiu, T.A.; Da, J.; Mensch, A.C.; Hamers, R.J.; Rosenzweig, Z.; Fairbrother, D.H.; et al. Investigation of Phosphorous Doping Effects on Polymeric Carbon Dots: Fluorescence, Photostability, and Environmental Impact. *Carbon* **2018**, *129*, 438–449. [[CrossRef](#)]
33. Boakye-Yiadom, K.O.; Kesse, S.; Opoku-Damoah, Y.; Filli, M.S.; Aquib, M.; Joelle, M.M.B.; Farooq, M.A.; Mavlyanova, R.; Raza, F.; Bavi, R.; et al. Carbon Dots: Applications in Bioimaging and Theranostics. *Int. J. Pharm.* **2019**, *564*, 308–317. [[CrossRef](#)]
34. Dhenadhayalan, N.; Lin, K.; Saleh, T.A. Recent Advances in Functionalized Carbon Dots toward the Design of Efficient Materials for Sensing and Catalysis Applications. *Small* **2020**, *16*, 1905767. [[CrossRef](#)]
35. Rajendran, S.; UshaVipinachandran, V.; Badagoppam Haroon, K.H.; Ashokan, I.; Bhunia, S.K. A Comprehensive Review on Multi-Colored Emissive Carbon Dots as Fluorescent Probes for the Detection of Pharmaceutical Drugs in Water. *Anal. Methods* **2022**, *14*, 4263–4291. [[CrossRef](#)] [[PubMed](#)]
36. Meng, W.; Bai, X.; Wang, B.; Liu, Z.; Lu, S.; Yang, B. Biomass-Derived Carbon Dots and Their Applications. *Energy Environ. Mater.* **2019**, *2*, 172–192. [[CrossRef](#)]
37. Dai, H. Carbon Nanotubes: Opportunities and Challenges. *Surf. Sci.* **2002**, *500*, 218–241. [[CrossRef](#)]
38. Li, X.; Yu, J.; Wageh, S.; Al-Ghamdi, A.A.; Xie, J. Graphene in Photocatalysis: A Review. *Small* **2016**, *12*, 6640–6696. [[CrossRef](#)]
39. Gao, J.; Zhu, M.; Huang, H.; Liu, Y.; Kang, Z. Advances, Challenges and Promises of Carbon Dots. *Inorg. Chem. Front.* **2017**, *4*, 1963–1986. [[CrossRef](#)]
40. Das, A. LED Light Sources in Organic Synthesis: An Entry to a Novel Approach. *Lett. Org. Chem.* **2022**, *19*, 283–292. [[CrossRef](#)]
41. Wang, C.; Sun, Z.; Zheng, Y.; Hu, Y.H. Recent Progress in Visible Light Photocatalytic Conversion of Carbon Dioxide. *J. Mater. Chem. A* **2019**, *7*, 865–887. [[CrossRef](#)]
42. Samanta, S.; Khilari, S.; Srivastava, R. Stimulating the Visible-Light Catalytic Activity of Bi₂MoO₆ Nanoplates by Embedding Carbon Dots for the Efficient Oxidation, Cascade Reaction and Photoelectrochemical O₂ Evolution. *ACS Appl. Nano Mater.* **2018**, *1*, 426–441. [[CrossRef](#)]
43. Majumdar, B.; Mandani, S.; Bhattacharya, T.; Sarma, D.; Sarma, T.K. Probing Carbocatalytic Activity of Carbon Nanodots for the Synthesis of Biologically Active Dihydro/Spiro/Glyco Quinazolinones and Aza-Michael Adducts. *J. Org. Chem.* **2017**, *82*, 2097–2106. [[CrossRef](#)] [[PubMed](#)]
44. Majumdar, B.; Sarma, D.; Jain, S.; Sarma, T.K. One-Pot Magnetic Iron Oxide–Carbon Nanodot Composite-Catalyzed Cyclooxidative Aqueous Tandem Synthesis of Quinazolinones in the Presence of Tert -Butyl Hydroperoxide. *ACS Omega* **2018**, *3*, 13711–13719. [[CrossRef](#)]
45. Manjupriya, R.; Roopan, S.M. Carbon Dots-Based Catalyst for Various Organic Transformations. *J. Mater. Sci.* **2021**, *56*, 17369–17410. [[CrossRef](#)]
46. Sui, G.; Li, J.; Du, L.; Zhuang, Y.; Zhang, Y.; Zou, Y.; Li, B. Preparation and Characterization of G-C₃N₄/Ag–TiO₂ Ternary Hollowsphere Nanoheterojunction Catalyst with High Visible Light Photocatalytic Performance. *J. Alloys Compd.* **2020**, *823*, 153851. [[CrossRef](#)]

47. Sun, H.; Zou, C.; Liao, Y.; Tang, W.; Huang, Y.; Chen, M. Modulating Charge Transport Behavior across the Interface via G-C₃N₄ Surface Discrete Modified BiOI and Bi₂MoO₆ for Efficient Photodegradation of Glyphosate. *J. Alloys Compd.* **2023**, *935*, 168208. [[CrossRef](#)]
48. Yoshinaga, T.; Iso, Y.; Isobe, T. Particulate, Structural, and Optical Properties of D-Glucose-Derived Carbon Dots Synthesized by Microwave-Assisted Hydrothermal Treatment. *ECS J. Solid State Sci. Technol.* **2018**, *7*, R3034–R3039. [[CrossRef](#)]
49. Alarfaj, N.; El-Tohamy, M.; Oraby, H. CA 19-9 Pancreatic Tumor Marker Fluorescence Immunosensing Detection via Immobilized Carbon Quantum Dots Conjugated Gold Nanocomposite. *Int. J. Mol. Sci.* **2018**, *19*, 1162. [[CrossRef](#)]
50. Geng, R.; Yin, J.; Zhou, J.; Jiao, T.; Feng, Y.; Zhang, L.; Chen, Y.; Bai, Z.; Peng, Q. In Situ Construction of Ag/TiO₂/g-C₃N₄ Heterojunction Nanocomposite Based on Hierarchical Co-Assembly with Sustainable Hydrogen Evolution. *Nanomaterials* **2019**, *10*, 1. [[CrossRef](#)]
51. Zhang, X.; Ren, B.; Li, X.; Liu, B.; Wang, S.; Yu, P.; Xu, Y.; Jiang, G. High-Efficiency Removal of Tetracycline by Carbon-Bridge-Doped g-C₃N₄/Fe₃O₄ Magnetic Heterogeneous Catalyst through Photo-Fenton Process. *J. Hazard. Mater.* **2021**, *418*, 126333. [[CrossRef](#)]
52. Anandan, S.; Wu, J.J.; Bahnemann, D.; Emeline, A.; Ashokkumar, M. Crumpled Cu₂O-g-C₃N₄ Nanosheets for Hydrogen Evolution Catalysis. *Colloids Surf. A Physicochem. Eng. Asp.* **2017**, *527*, 34–41. [[CrossRef](#)]
53. Xu, Q.; Jiang, C.; Cheng, B.; Yu, J. Enhanced Visible-Light Photocatalytic H₂-Generation Activity of Carbon/g-C₃N₄ Nanocomposites Prepared by Two-Step Thermal Treatment. *Dalt. Trans.* **2017**, *46*, 10611–10619. [[CrossRef](#)] [[PubMed](#)]
54. Zhu, Z.; Ma, C.; Yu, K.; Lu, Z.; Liu, Z.; Huo, P.; Tang, X.; Yan, Y. Synthesis Ce-Doped Biomass Carbon-Based g-C₃N₄ via Plant Growing Guide and Temperature-Programmed Technique for Degrading 2-Mercaptobenzothiazole. *Appl. Catal. B Environ.* **2020**, *268*, 118432. [[CrossRef](#)]
55. Yang, X.; Qian, F.; Zou, G.; Li, M.; Lu, J.; Li, Y.; Bao, M. Facile Fabrication of Acidified G-C₃N₄/g-C₃N₄ Hybrids with Enhanced Photocatalysis Performance under Visible Light Irradiation. *Appl. Catal. B Environ.* **2016**, *193*, 22–35. [[CrossRef](#)]
56. Kumar, A.; Raizada, P.; Singh, P.; Saini, R.V.; Saini, A.K.; Hosseini-Bandegharai, A. Perspective and Status of Polymeric Graphitic Carbon Nitride Based Z-Scheme Photocatalytic Systems for Sustainable Photocatalytic Water Purification. *Chem. Eng. J.* **2020**, *391*, 123496. [[CrossRef](#)]
57. Rohilla, S.; Gupta, A.; Kumar, V.; Kumari, S.; Petru, M.; Amor, N.; Dalal, J. Excellent UV-light triggered photocatalytic performance of ZnO.SiO₂ nanocomposite for water pollutant compound methyl orange dye. *Nanomaterials* **2021**, *11*, 2548. [[CrossRef](#)]
58. Aditya, M.N.; Chellapandi, T.; Prasad, G.K.; Venkatesh, M.J.P.; Khan, M.M.R.; Madhumitha, G.; Roopan, S.M. Biosynthesis of Rod Shaped Gd₂O₃ on g-C₃N₄ as Nanocomposite for Visible Light Mediated Photocatalytic Degradation of Pollutants and RSM Optimization. *Diam. Relat. Mater.* **2022**, *121*, 108790. [[CrossRef](#)]
59. Li, Y.; Sun, H.; Peng, T.; Qing, X. Effect of Temperature on the Synthesis of G-C₃N₄/Montmorillonite and Its Visible-Light Photocatalytic Properties. *Clays Clay Miner.* **2022**, *70*, 555–565. [[CrossRef](#)]
60. Chellapandi, T.; Madhumitha, G. Facile Synthesis and Characterization of Carrisa Edulis Fruit Extract Capped NiO on MK30 Surface Material for Photocatalytic Behavior against Organic Pollutants. *Mater. Lett.* **2023**, *330*, 133215. [[CrossRef](#)]
61. Chellapandi, T.; Roopan, S.M.; Madhumitha, G. Interfacial Charge Transfer of Carrisa Edulis Fruit Extract Capped Co₃O₄ Nanoparticles on the Surface of MK30: An Efficient Photocatalytic Removal of Methylthionium Chloride and Tetracycline Organic Pollutants. *Environ. Res.* **2022**, *219*, 115052. [[CrossRef](#)] [[PubMed](#)]
62. Shimi, A.K.; Parvathiraj, C.; Kumari, S.; Dalal, J.; Kumar, V.; Wabaidur, S.M.; Alothman, Z.A. Green synthesis of SrO nanoparticles using leaf extract of *Albizia julibrissin* and its recyclable photocatalytic activity: An eco-friendly approach for treatment of industrial wastewater. *Environ. Sci. Adv.* **2022**, *1*, 849–861. [[CrossRef](#)]
63. Ding, Y.; Lin, Z.; Deng, J.; Liu, Y.; Zhang, L.; Wang, K.; Xu, S.; Cao, S. Construction of Carbon Dots Modified Hollow G-C₃N₄ Spheres via in Situ Calcination of Cyanamide and Glucose for Highly Enhanced Visible Light Photocatalytic Hydrogen Evolution. *Int. J. Hydrog. Energy* **2022**, *47*, 1568–1578. [[CrossRef](#)]
64. Zhang, L.; Israel, E.M.; Yan, J.; Ritter, T. Copper-Mediated Etherification via Aryl Radicals Generated from Triplet States. *Nat. Synth.* **2022**, *1*, 376–381. [[CrossRef](#)]
65. Rosso, C.; Filippini, G.; Prato, M. Use of Nitrogen-Doped Carbon Nanodots for the Photocatalytic Fluoroalkylation of Organic Compounds. *Chem. Eur. J.* **2019**, *25*, 16032–16036. [[CrossRef](#)]
66. Meth-Cohn, O.; Narine, B.; Tarnowski, B. A Versatile New Synthesis of Quinolines and Related Fused Pyridines, Part 5. The Synthesis of 2-Chloroquinoline-3-Carbaldehydes. *J. Chem. Soc. Perkin Trans. 1* **1981**, 1520. [[CrossRef](#)]

Disclaimer/Publisher's Note: The statements, opinions and data contained in all publications are solely those of the individual author(s) and contributor(s) and not of MDPI and/or the editor(s). MDPI and/or the editor(s) disclaim responsibility for any injury to people or property resulting from any ideas, methods, instructions or products referred to in the content.